Fourier transform mid-infrared-attenuated total reflectance (FTMIR-ATR) microspectroscopy for determining textural property of microwave baked tuber

Su, Wen-Hao; Bakalis, Serafim; Sun, Da-Wen

DOI:
10.1016/j.jfoodeng.2017.08.016

Fourier transform mid-infrared-attenuated total reflectance (FTMIR-ATR) microspectroscopy for determining textural property of microwave baked tuber

Wen-Hao Su, Serafim Bakalis, Da-Wen Sun

PII: S0260-8774(17)30353-9

DOI: 10.1016/j.jfoodeng.2017.08.016

Reference: JFOE 8991

To appear in: *Journal of Food Engineering*

Received Date: 23 April 2017

Revised Date: 08 July 2017

Accepted Date: 17 August 2017

Please cite this article as: Wen-Hao Su, Serafim Bakalis, Da-Wen Sun, Fourier transform mid-infrared-attenuated total reflectance (FTMIR-ATR) microspectroscopy for determining textural property of microwave baked tuber, *Journal of Food Engineering* (2017), doi: 10.1016/j.jfoodeng.2017.08.016

Fourier transform mid-infrared-attenuated total reflectance (FTMIR-ATR) microspectroscopy for determining textural property of microwave baked tuber

Wen-Hao Su[a], Serafim Bakalis[b], Da-Wen Sun[a*]

[a] Food Refrigeration and Computerised Food Technology (FRCFT), School of Biosystems and Food Engineering, Agriculture & Food Science Centre, University College Dublin (UCD), National University of Ireland, Belfield, Dublin 4, Ireland

[b] School of Chemical Engineering, University of Birmingham, Edgbaston, Birmingham B15 2TT, UK

Abstract

Time series spectroscopic and textural analysis data were obtained from 5 varieties of tuber samples during microwave baking. These data were analyzed using evolutionary computing methods including partial least square discriminant analysis (PLSDA), partial least square regression (PLSR) and locally weighted partial least squares regression (LWPLSR). PLSDA was able to discriminate the tuber samples into three separate classes corresponding to their spectral properties. The predictability of spectra in full wavenumber region (4000–600 cm^{-1}) and fingerprint region (1500–900 cm^{-1}) were calculated using PLSR and LWPLSR and the relative performances of developed models were compared. It was observed that similar or even better predictions were obtained by models using spectra in the fingerprint region. Then, first-derivative and mean centering iteration algorithm (FMCIA) was carried out to select potential effective wavelengths and these selected wavelengths were further simplified using successive projections algorithm (SPA) for improving the model efficiency. Based on the FMCIA-SPA method for wavelength selection, the optimized models were established using LWPLSR for determination of tuber textural property (TTP) in terms of hardness,

[*] Corresponding author. Tel.: +353 1 7167342; Fax: +353 1 7167493.

E-mail address: dawen.sun@ucd.ie (D.-W. Sun).

URLs: http://www.ucd.ie/refrig, http://www.ucd.ie/sun (D.-W. Sun).

resilience, springiness, cohesiveness, gumminess and chewiness, with correlation coefficient of prediction (R_P) of 0.797, 0.881, 0.584, 0.574, 0.728 and 0.690, respectively. The results of this study demonstrated that FTMIR-ATR spectroscopy could be used reliably and rapidly for the non-destructive assessment of textural property of microwave baked tuber.

Keywords

FTMIR-ATR; Textural property; Potato; Multivariate regression; Non-destructive testing

1. Introduction

The tubers in terms of potato (*Solanum* Spp.) and sweet potato (*Ipomoea batatas* L.) are the primary staple food in many parts of the world (Villordon et al., 2014). The potato and sweet potato could provide more edible energy than many other staple foods. Since their higher moisture content (about 80%), the shelf-life of tuber products is relatively short (Saha et al., 2014). Thermal drying is considered as an effective way for preservation of tuber products. In the process of heat treating, the tuber sensory attribute would be affected by interactions of starch molecular with non-starch polysaccharides and sugars. Because of the starch gelatinization and retrogradation behaviour during thermal processing, the tuber textural property (TTP) could have many changes (Kim et al., 1997). For consumers, one of the most important quality attributes of tubers is the texture (Bordoloi et al., 2012). The food texture is normally defined as an integration of mechanical attributes of a food product perceptible relying on tactile, mechanical, visual and auditory receptors. As a critical sensory attribute, the texture of tuber product is mainly depended on its chemical compositions such as starch contents, non-starch polysaccharides, lignin and protein (Kita, 2002). The breakdown of tuber cell wall and middle lamellae structural components could have a great influence on the tuber texture (Alvarez and Canet, 1998). The textural parameters of tuber products mainly involve hardness, resilience, springiness, cohesiveness, gumminess and chewiness. However, the conventional detection methods for evaluation of tuber texture are based on appearance and taste, which is not only inaccurate but also time-consuming (Davies and Dixon, 1976). To eliminate the influence from human factors, the mechanical measurement methods such as texture profile analysis and the 3-point bending test have been proposed to detect the food texture (Fagan et al., 2007a). Nevertheless, the texture analyser with strong destructiveness and low efficiency is not the ideal solution. More importantly, both the sensory and instrumental evaluation approaches are suitable for sampling inspection, which means that only a small number of samples can be detected. However, the tuber industry requires a non-destructive and cost-effective technique for rapid and effective inspection of tuber texture.

Recently, some interesting approaches are based on the use of computer vision, nuclear magnetic resonance (NMR), biosensors, electronic noses, and vibrational spectroscopy methods to describe the quality of tuber products (Arkhypova et al., 2008; Biondi et al., 2014; Ding et al., 2015; Hansen et al., 2010; Pedreschi et al., 2011; Su and Sun, 2016d; Sun, 2016). In particular, for sensory analysis of tuber products, surface defects on potatoes and kinetics of color changes in potato slices were measured using computer vision systems (Pedreschi et al., 2006; Razmjooy et al., 2012). Due to the limitation of the charge coupled device (CCD) camera, the resolution of the common image was usually very low and the microstructure of the test sample cannot be obtained. Besides, the sensory texture attributes of cooked potatoes were assessed using NMR-imaging (Thybo et al., 2004). However, the sensory attributes such as graininess and mealiness could not be detected with this restricted technique. As another non-invasive and rapid spectroscopic technique, infrared (IR) spectroscopy can provide information about different food compositions at the same time and there is also no pre-treatment for sample preparation. Although near-infrared (NIR) spectroscopy is widely applied for food quality evaluation, the information given by NIR is based on molecular overtone and combination vibrations that are less sensitive and specific (Cen and He, 2007).

Fourier transform mid-infrared (FTMIR) spectroscopic technique is proved to provide more specific information than NIR sensors and has been successfully exploited for qualitative and quantitative analyses of food and food products (Alexandrakis et al., 2012; Karoui et al., 2010; Klaypradit et al., 2011; Su et al., 2015). The MIR spectroscopy monitors the vibrational and rotational motions of molecules in which very small differences in sample composition can be measured. As MIR spectra are rich in information on both physical states and molecular structures of food components, it allows for not only chemical determination of organic constituents but also physical identification of food texture property. MIR spectroscopy with attenuated total reflectance (ATR) has been identified as having considerable potential for real-time application in food industry. Many studies have investigated the potential of the IR spectroscopy to determine food sensory texture attributes including hardness, shear force, adhesiveness, chewiness, cohesiveness and springiness (Cai et al., 2011; Fagan et al., 2007a; Fagan et al., 2007b; Wu et al., 2014). However, there are few researches on measurement of textural property of tuber products using MIR spectroscopy.

The MIR region (4000–400 cm^{-1}) contains four broad continuous regions in terms of the X−H stretching region (4000−2500 cm^{-1}), the triple bond region (2500−2000 cm^{-1}), the double bond region (2000−1500 cm^{-1}), and the fingerprint region (1500−400 cm^{-1}) (Stuart, 2005). The numerous wavenumbers in the MIR region are irrelevant information for chemometrics analysis (Li et al., 2015). These redundant spectra need to be reduced and the survived spectra should be the most important wavenumbers. Some available methods such as genetic algorithms (GA), synergy interval partial least squares (SiPLS), backward interval partial least squares (biPLS), and competitive adaptive reweighted sampling (CARS) have been widely used for selection of feature wavenumbers in MIR region (Li et al., 2016; Wu et al., 2015). By selecting feature wavenumbers, both the model accuracy and detection efficiency could be improved. Our study sought to investigate the Fourier transform mid-infrared attenuated total reflectance (FTMIR-ATR) spectroscopic technique in quantitative prediction of the textural property of microwave baked tuber products. Spectral analysis of 125 samples from 5 tuber varieties at 5 time points was conducted. On the basis of the results, 6 different textural parameters including hardness, resilience, springiness, cohesiveness, gumminess and chewiness were evaluated by developing multivariate analytical methods. Then, the TTP was evaluated using a new spectral selection method. The ultimate objective of this study was to rapidly predict the TTP based on feature wavenumbers in the MIR region.

2. Materials and methods

2.1. Samples preparation

To develop a robust calibration model, fresh tuber samples from five types (25 samples for each type) in terms of Rooster red potato (origin: UK), Desiree red potato (origin: UK), Evangeline sweet potato (origin: Egypt), Abees sweet potato (origin: Egypt), organic Abees sweet potato (origin: Egypt) (GB-ORG-05 EU/non-EU agriculture) were purchased from large supermarkets in Birmingham, West Midlands, England. These samples were then transported to the freshness keeping compartment (about 4 °C, relative humidity 85%) at the laboratory of School of Chemical Engineering, University of Birmingham (UoB), UK, so as to reduce moisture loss and enzyme activity of tubers. After being peeled and sliced to the thickness of 10 mm (the axial length of 15 mm), 25 samples of each tuber variety were divided into five equal parts (5 samples for each part) and then respectively baked in a lab-scale microwave oven (800 W) for 0, 10, 20, 30, 35s, resulting in 125 samples (25 × 5) in total for five tuber varieties, eventually. Among them, 25 samples (5 samples from each tuber variety) were randomly selected as the prediction set, and the rest of 100 samples (20 samples of each time period) were used as the calibration set (group F). The samples in group F were divided into five equal groups based on the baking time (T1 for 0s, T2 for 10s, T3 for 20s, T4 for 30s and T5 for 35s). The samples of T1, T2 and T3 formed a new group G, and samples of T3, T4 and T5 combined another group H. Then, each sample was first scanned by a FT-IR spectral imaging system before the reference values of textural parameter being collected.

2.2 Data collection of FT-IR microspectral imaging system

The samples were analyzed using a LUMOS FT-IR microscope (Bruker Optics, Germany) in ATR mode (Cao et al., 2016; Woess et al., 2017). This system was equipped with a liquid nitrogen cooled narrow-band photoconductive mercury cadmium telluride (MCT) detector, a deuterated triglycine sulfate (DTGS) detector, a highly resolving digital CCD camera, a germanium (Ge) ATR crystal, a solid state laser, a IR beam splitter, and a permanently aligned RockSolidTM interferometer which was extremely insensitive against mirror tilts, vibrations and thermal effects. All components were motorized and electronically coded. The images of regions of interest were captured by the CCD camera. The aperture was 20 μm × 20 μm to obtain a high S/N ratio as well as a high spatial resolution, which allowed high quality MIR spectra to be acquired in the wavelength range of 2500–16680 nm (4000 to 600 cm^{-1}) at 4 cm^{-1} spectral resolution. Before each sample scan, a background scan was acquired with an empty sample plate. To remove any interference from the previous sample, the ATR crystal was cleaned using 70% ethanol and dried with a pure cotton fabric after each sample scan. Then, a total of 32 successive scans for each point of a sample were co-added and converted to absorbance based on the OPUS 7.2 software. More detailed information about the schema of the equipment as well as detector theory and technology can be found in the study of Bhargava and Levin (2008). Fig. 1B shows the representative microscopic images of Rooster tuber samples of 5 time periods from 0 to 35s. The spectra of 4 typical points from each sample were collected and averaged to represent that sample.

2.3 Textural property measurement

The textural property of a tuber sample was assessed by performing double compression test using a TA.XT.plus texture analyser (Stable Micro Systems Ltd., Godalming, Surrey, England) fitted with a 30 kg load cell. The force and height calibrations were executed prior to tests as these calibrations ensured that the measurements made by the Texture Analyser were accurate. In order to calculate the textural parameters accurately, the tests should be conducted with the same test and post-test speeds. Moreover, to replicate the biting action well, the diameter of compression plate used was larger than the diameter of tuber samples (15 mm) so that the tested samples can not only barrel out but also be fully contacted and properly compressed. In addition, different compression distances from the strain of 20% to 80% were tested to emulate the chewing action. It was found that the 40% strain was more appropriate to evaluate tuber samples after observing their behaviours. Therefore, each sample in this study was axially compressed twice to 40% deformation with a 40-mm diameter cylindrical aluminium plate at the pre-test speed of 2.0 mm/s, and the test and post-test speed of 1.0 mm/s, respectively. After the first compression, the plate returned to the trigger position. The trigger type was auto and the trigger force was 5.0 g. Besides, the interval between two compressions was 10 s. The acquisition of time data was 500 points per second. In this study, one tuber sample was first analysed by the FTMIR-ATR spectroscopic system and its textural property was then inspected using the texture analyser. After, the force–time deformation curve of the tuber sample could be displayed based on the fully integrated Texture Exponent 32-bit software in the computer. The textural parameters including hardness, resilience, springiness, cohesiveness, gumminess and chewiness could be acquired from the force–time deformation curve for analysis. According to such an operation process, both spectral data and textural parameters of all the five categories of tuber samples from 0s to 35s were collected. The specific definition and calculation of relevant mechanical parameters of texture can be found in the study of Trinh and Glasgow (2012). The statistics of these textural parameters are summarized in Table 1. The large variability of not lower than 0.226 suggested that the samples acquired in this study had strong representative and would be very helpful for the development of a robust model. Other textural parameters such as adhesiveness, stringiness and fracturability were not calculated in this test because of their intrinsic attributes.

2.4 Spectral pre-treatment

The obtained spectra mainly contained the tuber sample information but might involve systemic noises due to instrumental drift and light scattering. To develop an accurate spectroscopic model, the raw spectra should be corrected by applying mathematical pre-processing methods to reduce the undesirable information. In this study, spectral data were treated with four pre-processing methods: first derivative (1st Der) (7 points window, 2 order polynomial), second derivative (2nd Der) (7 points window, 2 order polynomial), orthogonal signal correction (OSC), and mean centering (MC) (Azzouz et al., 2003). Specifically, 2nd Der and OSC were first individually used to the data. Meanwhile, the methods of MC combined with both 1st Der and OSC were respectively applied. The optimal pre-processing technique would be survived when the lowest root mean square error of cross validation (RMSECV) and highest correlation coefficient (*R*) were acquired.

2.5 Feature wavenumber selection and optimization

The obtained FTMIR-ATR spectral data (4000 to 600 cm^{-1}) contain 1667 continuous wavenumbers. To accelerate data processing and enhance model robustness, spectral dimension reduction and uninformative wavelength elimination need to be carried out. The first-derivative and mean centering iteration algorithm (FMCIA) is a new efficient spectral selection approach that has been deeply utilized for detection of tuber quality based on NIR spectroscopy (Su and Sun, 2016a, c). In a recent study, the model performance was improved a lot using the wavelength selection method of regression coefficients (RC) combined with the FMCIA (Su and Sun, 2017). Moreover, successive projections algorithm (SPA) has been proved to be a more effective tool than RC for modelling and solving the collinearity problem (He et al., 2014). Detailed information about FMCIA and SPA can be found in other studies (Su and Sun, 2016b; Wu et al., 2012). In this study, FMCIA and SPA were combined to choose the most useful feature wavenumbers. Specifically, FMCIA was first applied to collect a batch of the common potential variables that were related to comprehensive internal characteristics of tuber samples. To explore the effectiveness of these selected spectra, SPA was then conducted to obtain the most effective wavenumber subsets from the potential feature variables selected based on FMCIA. It is recommended to use the variables that carry the most effective information to develop simplified models for rapid detection. To our knowledge, it is the first time to use the FMCIA-SPA method for spectral wavelength selection in IR spectra analysis.

2.6 Regression model development

Locally weighted partial least squares regression (LWPLSR) can be seen as a suitable strategy to estimate the nonlinear dependence relation between **X**-block (i.e., spectra) and **Y**-block (i.e., analyte concentrations), and to facilitate the selection of proper calibration sets. For each unknown sample to be predicted, local regression models are carried out using specific calibration equations to improve prediction accuracy by selecting a reduced set of calibration spectra providing similar features. The closest samples characterized by a minimum distance between the query and the calibration samples can be employed for local model calculation. This is on basis of using partial least squares regression (PLSR) algorithm to extract a set of latent variables (LVs) explaining the sources of variation of spectral signals correlated to sample composition. Normally, the database $\mathbf{X}$ ($p \times q$ matrix) in the calibration set of LWPLSR model consists of p samples where the kth sample X_k has q spectral variables selected to estimate the Y vectors. The query X_l is the sample whose concentration needs to be estimated.

$$\mathbf{X} = [\mathrm{X}_1\ \mathrm{X}_2\ \mathrm{X}_3 \ldots \mathrm{X}_q]^T \tag{1}$$

$$\mathbf{Y} = [\mathrm{Y}_1\ \mathrm{Y}_2\ \mathrm{Y}_3 \ldots \mathrm{Y}_p]^T \tag{2}$$

$$\mathrm{X}_k = [\mathrm{X}_{k1}\ \mathrm{X}_{k2}\ \mathrm{X}_{k3} \ldots \mathrm{X}_{kq}]^T \tag{3}$$

$$\mathrm{X}_l = [\mathrm{X}_{l1}\ \mathrm{X}_{l2}\ \mathrm{X}_{l3} \ldots \mathrm{X}_{lq}]^T \tag{4}$$

where T denotes the transpose of the matrix. In the LWPLSR, the similarity S_k between X_k and X_l is introduced to determine weights on samples in the calibration set.

$$\mathrm{S}_k = \exp\left(-\frac{\rho d_k}{\mu_d}\right) \qquad (\mathrm{k}=1, 2, 3\ldots, p) \tag{5}$$

$$\mathbf{S} = [\mathrm{S}_1\ \mathrm{S}_2\ \mathrm{S}_3 \ldots \mathrm{S}_p]^T \tag{6}$$

$$d_k = \sqrt{\sum_{\mathrm{t}=1}^{\mathrm{q}} (x_{k,t} - x_{l,t})^2} \tag{7}$$

$$\mathrm{d} = [\mathrm{d}_1\ \mathrm{d}_2\ \mathrm{d}_3 \ldots \mathrm{d}_p]^T \tag{8}$$

$$\bar{d} = \frac{1}{p}\sum_{k=1}^{p} d_k \tag{9}$$

$$\mu_d = \sqrt{\sum_{\mathrm{k}=1}^{\mathrm{p}} (d_k - \bar{d})^2/(p-1)} \tag{10}$$

where d denotes the distance vector, d_k represents the distance between X_k and X_l, ρ is the tuning parameter that can be determined by cross-validation, $\bar{d}$ is the mean distance, and μ_d is the standard deviation. The similarity S_k decreases in an exponential manner and approaches asymptotically to zero as the distance from the query increases. Moreover, S_k decreases more slowly as the parameter ρ is smaller. LWPLSR treats PLSR as a special case when $\rho = 0$ as $\mathrm{S}_k = 1$ for all samples. The sample size of the LWPLSR models varied between 10 and 300 in steps of 10. The optimal combination of the aforementioned parameters was selected from results obtained by a multi-parametric approach using the RMSECV as response function. The PLSR is commonly applied as statistical method for building linear regression model while the PLSDA is a supervised classification approach that can be applied to heighten the separation between groups of observations based on the PLSR (Su and Sun, 2016b). The response of Y-variable in PLSDA is a set of binary variables which is connected with the category of the sample. The latent variables (LVs) of these three PLS models were measured by venetian blinds cross-validation by mapping the number of factors against the RMSECV. The optimum number of LVs was determined by the lowest value of RMSECV. An excellent model must have higher *R* as well as lower RMSE.

2.7 Assessment of model accuracy

The performance of PLS models was assessed using *R* and RMSE in calibration (R_C, RMSEC), cross-validation (R_{CV}, RMSECV), and prediction (R_P, RMSEP). Other parameters such as sensitivity, specificity and classification error were employed to evaluate the performance of PLSDA models. In this usage, the sensitivity (also called the true positive rate) is defined as the possibility of distinguishing a sample as belonging to the interested class, while the specificity (also called the true negative rate) is defined as the probability of identifying a sample as not pertaining to the interested class. In other words, specificity quantifies the avoiding of false positives, as sensitivity does for false negatives. The above spectral analysis and multivariate modelling was performed using the Matlab R2016a software (The Mathworks Inc., Natick, MA, USA). In addition, the time-series variation of tuber texture property during microwave baking was analyzed using the software of IBM SPSS Statistics 24.0 version. The corresponding statistical significance of regression was assessed using a one-way analysis of variance (ANOVA). *P*-values were calculated for each model, and the level of significance was assigned to probability lower than 0.05.

3. Result and discussion

3.1 Texture analysis of baked tuber

The connections of average reference values of TTP at five time points were described with curves in Fig. 2. To develop robust calibration models for tuber textural analysis, five different categories of fresh sweet potato and red potato tuber samples were investigated in this study. It was found that the hardness of sweet potato (Fig. 2a) was smaller than the red potato (Fig. 2g) in the beginning, but the larger gumminess and chewiness (Fig. 2e and f) were obtained by the sweet potato and the final values of these parameters were almost equivalent in the end. This demonstrated that the tuber products both sweet potato and red potato were fully cooked at 35 s. For the cohesiveness (Fig. 2c and i), the larger values were obtained by the sweet potato throughout the process. Nevertheless, the similarity of variation tendency of these six textural parameters between sweet potato (Fig. 2a-f) and red potato (Fig. 2g-i) was noticed. Accordingly, wide applicability models should be established based on all these tuber samples. The statistics of estimated models for textural analysis of tuber samples during microwave baking was summarized in Table 2.

3.2 Spectral feature of tuber samples

The average spectral data of micro-FTMIR-ATR of all samples obtained from various time points are depicted in Fig. 3a. As can be seen, the spectral trends (4000–600 cm^{-1}) of time-series samples (0–35s) are similar, but the distinct amplitude of spectra caused by the baking time of tuber samples are realized. The inspection of chemical species of tuber in characteristic spectra has been illustrated. The absorption peaks of wide bands at 3750–2800 cm^{-1} and 1800–1500 cm^{-1} were ascribed to the effect of strong water absorption due to O–H stretching vibrations (Ayvaz et al., 2016). This indicated that the decrease of spectral amplitude from 0 to 35s in these two regions was due to the loss of tuber moisture. Fig. 3b presents the magnified energy absorbance information associated with different kinds of functional groups. It was found that the spectral region of 1500 to 900 cm^{-1} is of greatest importance for the recognition of molecular structure (Lu and Rasco, 2012). For instance, the infrared absorptivity at 1345 cm^{-1}, 1357 cm^{-1}, 1429 cm^{-1} were related to asparagine and glutamine corresponding to C–H deformation, C–N stretches and C–H deformation, respectively. Besides, the region of 1200 cm^{-1}–1000 cm^{-1} which is associated with C–C ring vibrations, overlapped with the stretching vibrations of C–O–H side groups and the C–O–C glycosidic band vibrations of carbohydrates (Barth, 2000). In addition, the glucose was associated with bands at 1015 cm^{-1}, and the unconspicuous absorption band at 1062 cm^{-1} was assigned to C-O stretch vibration (Wilkerson et al., 2013). This indicated that the fingerprint spectra in the region of 1500 to 900 cm^{-1} may be more closely related to the tuber texture. Therefore, there is a need to develop regression models in both the full wavenumber region (4000–600 cm^{-1}) and the fingerprint region (1500-900 cm^{-1}) to study all kinds of tuber mechanical parameters.

3.3 PLSDA model for evaluation of spectral property

The spectral property of baked tuber was investigated based on PLSDA algorithm using raw spectra and OSC pus MC pre-treatment. To extract spectral features of PLSDA, the optimum numbers of LVs were determined based on the minimum values of RMSECV statistic. The obtained identification results of targeted class (T1-T5) in three modes (F, G and H) are tabulated in Table 3, where the performance of PLSDA is assessed by model parameters such as the sensitivity, specificity, classification error and R_{CV} for each class. For identification of T1 and T2, the performances of all models developed based on F and G were very good, and the highest accuracy was obtained in T1 followed by T2, which demonstrated that the spectra from T1 and T2 were easier to be distinguished from all the spectral data. This situation was mainly due to the higher tuber moisture content in T1 and T2. The larger moisture loss in T2 resulted in a bigger gap between T1 and T2. On the contrary, PLSDA models generated a very bad recognition of samples in T4 from the mode H, with the lowest accuracy values (R_{CV} = 0.130-0.226, RMSECV = 0.575-0.584). This indicated that the spectral property in T4 was more similar to that in T3 and T5 because of the little moisture loss in the late period of baking. Nevertheless, the models developed using pre-processing method showed better classification power than raw spectral model, apart from the detection of class T3 in mode F (R_{CV} = 0.333). Based on the PLSDA using pre-treatment method to classify T3, the accuracy (R_{CV} = 0.684) acquired in the mode G had more than doubled in comparison to the mode F and was higher than the mode H as well. The results showed that the small spectral variation can be revealed using the PLSDA with proper pre-treatment, and all the tuber samples in mode G can be discriminated into three separate clusters (T1, T2 and T3) with better effect corresponding to their spectral properties. The optimal results obtained from PLSDA models for evaluation of spectral property were clearly plotted using curves as shown in Fig. 4.

3.4 Detection of TTP using PLSR in the full-wavenumber region

FTMIR-ATR technique allowed the development of calibration models for quantification of TTP. The cross-validated PLSR models were developed to determine the textural properties in various tuber products based on the chemical information from their spectra. To evaluate the applicability of the proposed PLSR for the measurement of TTP, an independent set of samples was then assessed using a predicted PLSR model. All kinds of spectral pre-treatment algorithms were adopted to remove both additive and multiplicative noise effects in the spectra and improve the accuracy of the developed models. The detailed statistical parameters when constructed using the FT-IR raw spectra and various pre-treatment approaches are described in Table 4. The effects of spectral pre-processing algorithms on performances of PLSR models were inspected. It was found that the generated models using the OSC plus MC-corrected spectral data with MC in Y-block presented the best performance for prediction of hardness, resilience, springiness and gumminess, with R_P of 0.846, 0.893, 0.563 and 0.798, respectively. Although the spectra processed only by the OSC plus MC without Y-block MC provided similar R statistics in PLSR, the RMSEC, RMSECV and RMSEP were almost doubled. Besides, the PLSR with 2nd Der provided the best prediction model to determine the tuber cohesiveness. However, it was realized that the 2nd Der of the MIR spectra lowered the accuracy of PLSR model for the detection of resilience, probably because the spectra contained the interfering variance which was increased using this data pre-processing. In addition, the highest accuracy (R_P = 0.797, RMSEP=34.598) for measuring chewiness was existed in the PLSR model developed using the OSC, followed by the spectral pre-processing method of OSC plus MC (in X-block) with another MC in Y-block. Overall, the model performance can be fully improved based on optimal pre-treatment algorithms (Fig. 5). Moreover, the most optimal pre-processing methods were acquired by the OSC plus MC-corrected spectra with MC in Y-block, providing more precise predictions when compared to other pre-processing approaches.

3.5 Improving the measuring accuracy of TTP using LWPLSR

Although a good correlation between the IR spectral features and the TTP reference values has been presented in the PLSR, the detection accuracy still needs to be improved to meet the requirement of the advanced food processing. Based on the optimal pre-processing method, the LWPLSR model was then constructed to study the correlation between the FTMIR-ATR spectra and textural property reference values acquired at five different time points. The parameters of LWPLSR models using raw spectra and the OSC plus MC-corrected spectra with MC in Y-block are shown in Table 5. For determination of tuber springiness using LWPLSR model, the better performance (R_P = 0.520, RMSEP = 0.114) was obtained based on the spectral data without pre-processing, which was lower than the capacity of PLSR model using the OSC plus MC-corrected spectra with MC in Y-block. Nevertheless, it was found that the best calibration models for prediction of other five textural properties were acquired by employing the pre-processing method, and the R_P values were 0.878 for hardness, 0.911 for resilience, 0.666 for cohesiveness, 0.815 for gumminess and 0.817 for chewiness, respectively. Based on the LWPLSR model, these five coefficients being used to predict tuber textural properties were comparatively higher than the R_P values collected from PLSR models with the exception of the R_P for cohesiveness. This indicated that the PLSR model could obtain higher efficiency for evaluating tuber cohesiveness and springiness, although better detection accuracy of other four textural parameters were acquired in the LWPLSR model. Therefore, the accuracy of quantitative detection of TTP can be further optimized by combining the full-wavenumber PLSR with LWPLSR model (Fig. 6).

3.6 Analysis of TTP using the fingerprint region

Based on the analysis of optimal models in the full wavenumber range (4000–600 cm^{-1}), the results of PLSR and LWPLSR for measuring TTP using the confining spectra in the fingerprint region of 1500–900 cm^{-1} are described in Table 6. Coincidentally, the optimal prediction ability for measuring hardness, resilience, gumminess and chewiness was achieved using the fingerprint-wavenumber LWPLSR model, and other two parameters including cohesiveness and springiness were inspected with better accuracy in the fingerprint-wavenumber PLSR model. Compared with the performance of full-wavenumber models, the models using spectra in the narrow wavenumber range showed similar or even better capacity. This demonstrated that the calibration models developed in this study were robust and stabilized. Moreover, it was evident that the spectra without pre-processing offered an enhancement in the model accuracy of LWPLSR for detection of tuber hardness (R_P = 0.845), resilience (R_P = 0.909) and cohesiveness (R_P = 0.787). Although there was a deteriorative impact on the model predictability for assessing tuber springiness, gumminess and chewiness without spectral pre-treatment, the optimized models were found by using OSC plus MC in X-block with another MC in Y-block, with the R_P of 0.748, 0.814 and 0.742, respectively. Furthermore, the OSC plus MC spectral pre-treatment method provided the highest accuracy for inspection of tuber springiness. Using only 4 LVs, this fingerprint-wavenumber PLSR model yielded the highest R_P of 0.748 and similar RMSEP of 0.112 in comparison with other models. It was seen that none of other models showed the R_P higher than 0.600, which meant the simplified fingerprint-wavenumber models were more convenient.

3.7 Modelling with feature wavenumbers for determination of TTP

Even though the wavenumber quantity in the spectral region of 1500-900 cm^{-1} accounted for about 17.756% of the total spectra (1667), these almost 300 wavenumbers were still very redundant and affected the rapid measurement of TTP. To improve the TTP detection efficiency, a dozen of feature wavenumbers (1468, 1350, 1333, 1315, 1221, 1185, 1160, 1130, 1083, 1026, 985 and 924 cm^{-1}) were selected using FMCIA as described in Fig. 7a. On basis of chosen characteristic wavenumbers, the performances of simplified PLSR and LWPLSR calibration models were summarized in Table 7. As can be seen, the feature-wavenumber LWPLSR model provided the best results for all tuber textural parameters including hardness, resilience, cohesiveness, springiness, gumminess and chewiness compared to the PLSR. It was realized that the accuracy of the FMCIA-LWPLSR models (mean R_P = 0.760) performed slightly less superior than those optimal models (mean R_P = 0.808) established in the fingerprint region (1500–900 cm^{-1}). However, it was worth mentioning that FMCIA-LWPLSR models performed an acceptable result considering the largely reduced number of variables (95.946%). To explore the effectiveness of the most useful spectra in these twelve spectral wavebands, the number of characteristic wavenumber was further reduced and optimized based on the SPA. As shown in Fig. 7(b, c and d), three combinations of most important wavenumbers including (1350, 1221, 1083, 1026, 985, 924), (1468, 1333, 1221, 1026, 985, 924) and (1468, 1333, 1083, 1026, 985, 924) are indicated by square marker based on the combined FMCIA-SPA to predict these six textural parameters of tested samples. Finally, the FMCIA-SPA-LWPLSR models were established for TTP detection with the mean R_P of 0.709. The results presented in Fig. 8 revealed that performances of the evolutionary

LWPLSR models using six selected wavenumbers were comparable to those models developed using twelve wavenumbers, indicating that the method for wavelength selection using the FMCIA-SPA method was efficient.

3.8 Discussion

To develop a more robust calibration model for TTP determination, representative samples from various tuber varieties and different microwave baking degrees were acquired to generate large variability of tuber textural parameters. Based on 1667 wavenumbers in the full spectral range (4000–600 cm^{-1}), textural parameters of tuber samples including hardness, resilience, springiness, cohesiveness, gumminess and chewiness were respectively evaluated, with the highest mean R_P of 0.786. Many researches have emphasized the similar detection results of MIR spectroscopy using the spectra in both the full wavenumber region and the fingerprint region for assessing food quality (Karoui et al., 2010). Specifically, based on FTMIR spectroscopy and PLSR model to evaluate onion powder adulterant, the determination coefficients for prediction (R_p^2) of 0.90 and 0.89 were obtained for the full spectral and fingerprint regions, respectively (Lohumi et al., 2014). It was realized that food texture was closely bound up with its structure that was the characterization of spectra in the fingerprint region (Ricci et al., 2015). When 3 combinations of 6 feature wavenumbers in the fingerprint region (1500-900 cm^{-1}) were utilized in our research, the optimal mean R_P of 0.709 was achieved. Although the model accuracy had a slight reduction of 9.796%, the total amount of wavenumber reduced by 99.640% using the new wavenumber selection approach of FMCIA-SPA. The prediction results based on the FMCIA-SPA found in this research were better than those mentioned by Wu et al. (2014) and Pan et al. (2016) for measuring texture properties of other food products using wavelength selection methods such as RC and uninformative variable elimination (UVE) although more feature spectral data were employed in their studies. In a recent study of Li et al. (2016), 18 characteristic wavenumbers were eventually selected from the MIR spectral region to develop linear and nonlinear determination models. Fortunately, there were 12 feature wavenumbers chosen in our study based on the FMCIA, and just 6 characteristic wavenumbers left using the FMCIA-SPA. Accordingly, the FTMIR has a great potential in the near future as a high-efficiency technique for real-time determination of the integrated quality of complex food systems along with the development of sensors and chemometric algorithms.

4. Conclusions

In this study, the feasibility of MIR spectroscopy for the evaluation of TTP was investigated. The FTMIR-ATR spectroscopy provided characteristic information allowing a better understanding of the change of tuber texture under various microwave baking time. The FMCIA-SPA was first used to choose optimal feature wavenumbers based on spectroscopic technique. With only 6 most important wavenumbers selected from 1667 wavenumbers in the MIR region (4000–600 cm^{-1}), the performance of FMCIA-SPA-LWPLSR model was comparable to the optimal full-wavenumber models. The result of this study revealed that FTMIR-ATR spectroscopy can be considered as an effective technique for non-invasive and rapid measurement of textural property of tuber products. In the future research, more tuber samples from different varieties and origins will be investigated based on various spectroscopic techniques to verify the effectiveness of developed new chemometric algorithms.

Acknowledgments

The authors would like to acknowledge the ERASMUS plus programme of quantitative tools for sustainable food and energy in the food chain (Q-Safe) (Project No: 2014-1-MT01-KA200-000327) supported by European Union, and the UCD-CSC Scholarship Scheme supported by of University College Dublin (UCD) and China Scholarship Council (CSC).

References

Alexandrakis, D., Downey, G., Scannell, A.G., (2012). Rapid non-destructive detection of spoilage of intact chicken breast muscle using near-infrared and Fourier transform mid-infrared spectroscopy and multivariate statistics. Food and Bioprocess Technology 5(1), 338-347.

Alvarez, M.D., Canet, W., (1998). Rheological characterization of fresh and cooked potato tissues (cv. Monalisa). Zeitschrift für Lebensmitteluntersuchung und-Forschung A 207(1), 55-65.

Arkhypova, V., Dzyadevych, S., Jaffrezic-Renault, N., Martelet, C., Soldatkin, A., (2008). Biosensors for assay of glycoalkaloids in potato tubers. Applied Biochemistry and Microbiology 44(3), 314-318.

Ayvaz, H., Bozdogan, A., Giusti, M.M., Mortas, M., Gomez, R., Rodriguez-Saona, L.E., (2016). Improving the screening of potato breeding lines for specific nutritional traits using portable mid-infrared spectroscopy and multivariate analysis. Food Chemistry 211, 374-382.

Azzouz, T., Puigdoménech, A., Aragay, M., Tauler, R., (2003). Comparison between different data pre-treatment methods in the analysis of forage samples using near-infrared diffuse reflectance spectroscopy and partial least-squares multivariate calibration method. Analytica Chimica Acta 484(1), 121-134.

Barth, A., (2000). The infrared absorption of amino acid side chains. Progress in Biophysics and Molecular Biology 74(3), 141-173.

Bhargava, R., Levin, I.W., (2008). *Spectrochemical Analysis using Infrared Multichannel Detectors*. John Wiley & Sons.

Biondi, E., Blasioli, S., Galeone, A., Spinelli, F., Cellini, A., Lucchese, C., Braschi, I., (2014). Detection of potato brown rot and ring rot by electronic nose: From laboratory to real scale. Talanta 129, 422-430.

Bordoloi, A., Kaur, L., Singh, J., (2012). Parenchyma cell microstructure and textural characteristics of raw and cooked potatoes. Food Chemistry 133(4), 1092-1100.

Cai, J., Chen, Q., Wan, X., Zhao, J., (2011). Determination of total volatile basic nitrogen (TVB-N) content and Warner–Bratzler shear force (WBSF) in pork using Fourier transform near infrared (FT-NIR) spectroscopy. Food Chemistry 126(3), 1354-1360.

Cao, X., Loussaert, J.A., Wen, Z.-q., (2016). Microspectroscopic investigation of the membrane clogging during the sterile filtration of the growth media for mammalian cell culture. Journal of Pharmaceutical and Biomedical Analysis 119, 10-15.

Cen, H., He, Y., (2007). Theory and application of near infrared reflectance spectroscopy in determination of food quality. Trends in Food Science & Technology 18(2), 72-83.

Davies, H., Dixon, N., (1976). Evaluation of potato texture by taste and by appearance. American Journal of Potato Research 53(6), 205-210.

Ding, X., Ni, Y., Kokot, S., (2015). NIR spectroscopy and chemometrics for the discrimination of pure, powdered, purple sweet potatoes and their samples adulterated with the white sweet potato flour. Chemometrics and Intelligent Laboratory Systems 144, 17-23.

Fagan, C.C., Everard, C., O'Donnell, C., Downey, G., Sheehan, E., Delahunty, C., O'Callaghan, D., (2007a). Evaluating mid-infrared spectroscopy as a new technique for predicting sensory texture attributes of processed cheese. Journal of Dairy Science 90(3), 1122-1132.

Fagan, C.C., Everard, C., O'Donnell, C., Downey, G., Sheehan, E., Delahunty, C., O'Callaghan, D., Howard, V., (2007b). Prediction of processed cheese instrumental texture and meltability by mid-infrared spectroscopy coupled with chemometric tools. Journal of Food Engineering 80(4), 1068-1077.

Hansen, C.L., Thybo, A.K., Bertram, H.C., Viereck, N., van den Berg, F., Engelsen, S.B., (2010). Determination of dry matter content in potato tubers by low-field nuclear magnetic resonance (LF-NMR). Journal of Agricultural and Food Chemistry 58(19), 10300-10304.

He, H.-J., Wu, D., Sun, D.-W., (2014). Potential of hyperspectral imaging combined with chemometric analysis for assessing and visualising tenderness distribution in raw farmed salmon fillets. Journal of Food Engineering 126, 156-164.

Karoui, R., Downey, G., Blecker, C., (2010). Mid-infrared spectroscopy coupled with chemometrics: A tool for the analysis of intact food systems and the exploration of their molecular structure− Quality relationships− A review. Chemical Reviews 110(10), 6144-6168.

Kim, Y.S., Wiesenborn, D.P., Grant, L.A., (1997). Pasting and thermal properties of potato and bean starches. Starch ‐ Stärke 49(3), 97-102.

Kita, A., (2002). The influence of potato chemical composition on crisp texture. Food Chemistry 76(2), 173-179.

Klaypradit, W., Kerdpiboon, S., Singh, R.K., (2011). Application of artificial neural networks to predict the oxidation of menhaden fish oil obtained from Fourier transform infrared spectroscopy method. Food and Bioprocess Technology 4(3), 475-480.

Li, X., Sun, C., Luo, L., He, Y., (2015). Determination of tea polyphenols content by infrared spectroscopy coupled with iPLS and random frog techniques. Computers and Electronics in Agriculture 112, 28-35.

Li, X., Zhang, Y., He, Y., (2016). Rapid detection of talcum powder in tea using FT-IR spectroscopy coupled with chemometrics. Scientific Reports 6.

Lohumi, S., Lee, S., Lee, W.-H., Kim, M.S., Mo, C., Bae, H., Cho, B.-K., (2014). Detection of starch adulteration in onion powder by FT-NIR and FT-IR spectroscopy. Journal of Agricultural and Food Chemistry 62(38), 9246-9251.

Lu, X., Rasco, B.A., (2012). Determination of antioxidant content and antioxidant activity in foods using infrared spectroscopy and chemometrics: a review. Critical Reviews in Food Science and Nutrition 52(10), 853-875.

Pan, L., Lu, R., Zhu, Q., Tu, K., Cen, H., (2016). Predict compositions and mechanical properties of sugar beet using hyperspectral scattering. Food and Bioprocess Technology 9(7), 1177-1186.

Pedreschi, F., Leon, J., Mery, D., Moyano, P., (2006). Development of a computer vision system to measure the color of potato chips. Food Research International 39(10), 1092-1098.

Pedreschi, F., Mery, D., Bunger, A., Yanez, V., (2011). Computer vision classification of potato chips by color. Journal of Food Process Engineering 34(5), 1714-1728.

Razmjooy, N., Mousavi, B.S., Soleymani, F., (2012). A real-time mathematical computer method for potato inspection using machine vision. Computers & Mathematics with Applications 63(1), 268-279.

Ricci, A., Parpinello, G.P., Olejar, K.J., Kilmartin, P.A., Versari, A., (2015). Attenuated total reflection mid-infrared (ATR-MIR) spectroscopy and chemometrics for the identification and classification of commercial tannins. Applied Spectroscopy 69(11), 1243-1250.

Saha, A., Gupta, R.K., Tyagi, Y.K., (2014). Effects of edible coatings on the shelf life and quality of potato (Solanum tuberosum L.) tubers during storage. Journal of Chemical & Pharmaceutical Research 6(12).

Stuart, B., (2005). *Infrared Spectroscopy*. Wiley Online Library.

Su, W.-H., He, H.-J., Sun, D.-W., (2015). Non-destructive and Rapid Evaluation of Staple Foods Quality by Using Spectroscopic Techniques: A Review. Critical Reviews in Food Science and Nutrition(just-accepted), 00-00.

Su, W.-H., Sun, D.-W., (2016a). Comparative assessment of feature-wavelength eligibility for measurement of water binding capacity and specific gravity of tuber using diverse spectral indices stemmed from hyperspectral images. Computers and Electronics in Agriculture 130, 69-82.

Su, W.-H., Sun, D.-W., (2016b). Facilitated wavelength selection and model development for rapid determination of the purity of organic spelt (Triticum spelta L.) flour using spectral imaging. Talanta 155, 347-357.

Su, W.-H., Sun, D.-W., (2016c). Multivariate analysis of hyper/multi-spectra for determining volatile compounds and visualizing cooking degree during low-temperature baking of tubers. Computers and Electronics in Agriculture 127, 561-571.

Su, W.-H., Sun, D.-W., (2016d). Potential of hyperspectral imaging for visual authentication of sliced organic potatoes from potato and sweet potato tubers and rapid grading of the tubers according to moisture proportion. Computers and Electronics in Agriculture 125, 113-124.

Su, W.-H., Sun, D.-W., (2017). Evaluation of spectral imaging for inspection of adulterants in terms of common wheat flour, cassava flour and corn flour in organic Avatar wheat (Triticum spp.) flour. Journal of Food Engineering 200, 59-69.

Sun, D.-W., (2016). *Computer Vision Technology for Food Quality Evaluation*. Academic Press.

Thybo, A.K., Szczypiński, P.M., Karlsson, A.H., Dønstrup, S., Stødkilde-Jørgensen, H.S., Andersen, H.J., (2004). Prediction of sensory texture quality attributes of cooked potatoes by NMR-imaging (MRI) of raw potatoes in combination with different image analysis methods. Journal of Food Engineering 61(1), 91-100.

Trinh, K.T., Glasgow, S., (2012). On the texture profile analysis test. Chemeca 2012: Quality of life through chemical engineering: 23-26 September 2012, Wellington, New Zealand, 749.

Villordon, A.Q., Ginzberg, I., Firon, N., (2014). Root architecture and root and tuber crop productivity. Trends in plant science 19(7), 419-425.

Wilkerson, E.D., Anthon, G.E., Barrett, D.M., Sayajon, G.F.G., Santos, A.M., Rodriguez-Saona, L.E., (2013). Rapid assessment of quality parameters in processing tomatoes using hand-held and benchtop infrared spectrometers and multivariate analysis. Journal of Agricultural and Food Chemistry 61(9), 2088-2095.

Woess, C., Unterberger, S.H., Roider, C., Ritsch-Marte, M., Pemberger, N., Cemper-Kiesslich, J., Hatzer-Grubwieser, P., Parson, W., Pallua, J.D., (2017). Assessing various Infrared (IR) microscopic imaging techniques for post-mortem interval evaluation of human skeletal remains. PloS one 12(3), e0174552.

Wu, D., Shi, H., Wang, S., He, Y., Bao, Y., Liu, K., (2012). Rapid prediction of moisture content of dehydrated prawns using online hyperspectral imaging system. Analytica Chimica Acta 726, 57-66.

Wu, D., Sun, D.-W., He, Y., (2014). Novel non-invasive distribution measurement of texture profile analysis (TPA) in salmon fillet by using visible and near infrared hyperspectral imaging. Food Chemistry 145, 417-426.

Wu, Z., Xu, E., Long, J., Wang, F., Xu, X., Jin, Z., Jiao, A., (2015). Use of Attenuated Total Reflectance Mid‐Infrared Spectroscopy for Rapid Prediction of Amino Acids in Chinese Rice Wine. Journal of Food Science 80(8), C1670-C1679.

Table 1. Reference values of textural property of all tuber samples during microwave baking.

Textural parameter	Max	Min	Range	Mean ± SD	Variability
Hardness (N)	368.219	6.926	361.293	108.963± 105.352	0.967
Resilience	0.726	0.101	0.625	0.285±0.128	0.449
Cohesiveness	0.894	0.035	0.859	0.410±0.175	0.427
Springiness	0.867	0.120	0.747	0.562±0.127	0.226
Gumminess (N)	311.486	2.683	308.803	48.524±62.406	1.287
Chewiness (N)	223.363	1.320	222.043	31.157±44.798	1.438

SD: Standard Deviation, Variability = SD value/Mean value.

Table 2. Summary statistics of estimated models for textural analysis of tuber samples during microwave baking [a].

Mode Type	Targeted class detection	Calibration: Coefficients t^2	Calibration: Coefficients t (1/t)	Calibration: Coefficients Constant	Calibration: Equation ($0 \le t \le 35$ s)	Cross-validation: ANOVA Mean Square	Cross-validation: ANOVA *F* statistic	Cross-validation: ANOVA *p*-value	Cross-validation: *R*
Sweet potato tubers	Hardness	0.238 (0.008)	-15.069 (0.282)	266.333 (2.046)	$Y = 0.238t^2 - 15.069t + 266.333$	20266.558	4459.238	0.000	1.000 (2.132)
	Resilience	0.000 (0.000)	-0.005 (0.001)	0.37 (0.029)	$Y = -0.005t + 0.37$	0.018	13.884	0.034	0.907 (0.036)
	Cohesiveness	0.003 (0.000)	-0.057 (0.000)	0.678 (0.000)	$Y = 0.003t^2 - 0.057t + 0.678$ ($0 \le t \le 20$ s)	0.032	-	-	1.000 (0.000)
		0.010 (0.000)	-0.057 (0.000)	1.602 (0.000)	$Y = 0.010t^2 - 0.057t + 1.602$ ($20 < t \le 35$ s)	0.018	-	-	1.000 (0.000)
	Springiness	0.000 (0.000)	-0.006 (0.001)	0.656 (0.033)	$Y = -0.006t + 0.656$	0.030	18.250	0.024	0.927 (0.041)
	Gumminess	0.000 (0.000)	622.787 (5.495)	-3.83 (0.330)	$Y = 622.787/t - 3.830$	1241.757	12844.988	0.000	1.000 (0.311)
	Chewiness	0.179 (0.044)	-9.427 (1.615)	123.03 (11.722)	$Y = 0.179t^2 - 9.427t + 123.030$	5140.348	34.455	0.028	0.986 (12.214)
		0.000 (0.008)	395.631 (24.757)	-5.354 (1.487)	$Y = 395.631/t + 5.354$	501.115	255.376	0.004	0.996 (1.401)
Red potato tubers	Hardness	0.321 (0.055)	-19.646 (2.029)	319.428 (14.728)	$Y = 0.321t^2 - 19.646t + 319.428$	32150.036	136.528	0.007	0.996 (15.345)
	Resilience	0.0005 (0.000)	-0.009 (0.000)	0.327 (0.000)	$Y = 0.0005t^2 - 0.009t + 0.327$ ($0 \le t \le 20$ s)	0.001	-	-	1.000 (0.000)
		0.003 (0.000)	-0.155 (0.000)	2.354 (0.000)	$Y = 0.003t^2 - 0.155t + 2.354$ ($20 < t \le 35$ s)	0.008	-	-	1.000 (0.000)
	Cohesiveness	0.0004 (0.000)	-0.013 (0.002)	0.302 (0.016)	$Y = 0.0004t^2 - 0.013t + 0.302$	0.007	27.159	0.036	0.982 (0.016)
	Springiness	0.000 (0.000)	-0.005 (0.282)	0.683 (0.055)	$Y = -0.005t + 0.683$	0.019	4.119	0.135	0.761 (0.069)
	Gumminess	0.135 (0.020)	-7.176 (0.282)	96.78 (5.425)	$Y = 0.135t^2 - 7.176t + 96.780$	3053.539	95.573	0.010	0.995 (2.132)
	Chewiness	0.088 (0.010)	-4.625 (0.354)	60.617 (2.811)	$Y = -0.088t^2 - 4.625t + 60.617$	1625.673	144.643	0.007	0.997 (3.352)

[a] Standard errors in parentheses below coefficient estimates.

					Sensitivity	Specificity	Class. Error	R_C	RMSEC	Sensitivity	Specificity	Class. Error	R_{CV}	RMSECV
F	T1	None	None	10	0.960	0.920	0.065	0.831	0.224	0.940	0.880	0.090	0.729	0.285
		OSC+MC	MC	10	1.000	1.000	0.000	0.941	0.136	0.980	0.960	0.030	0.857	0.221
	T2	None	None	8	0.800	0.880	0.160	0.703	0.284	0.680	0.890	0.215	0.620	0.317
		OSC+MC	MC	8	0.920	0.960	0.060	0.825	0.226	0.760	0.890	0.175	0.643	0.322
	T3	None	None	8	0.720	0.770	0.230	0.506	0.354	0.560	0.770	0.335	0.333	0.385
		OSC+MC	MC	10	0.880	0.900	0.110	0.707	0.283	0.720	0.770	0.255	0.329	0.435
	T4	None	None	9	0.760	0.680	0.280	0.474	0.352	0.680	0.670	0.325	0.263	0.401
		OSC+MC	MC	7	0.920	0.900	0.090	0.713	0.28	0.680	0.770	0.275	0.321	0.430
	T5	None	None	10	0.720	0.850	0.215	0.620	0.314	0.600	0.790	0.305	0.438	0.374
		OSC+MC	MC	5	0.920	0.950	0.066	0.786	0.247	0.760	0.790	0.225	0.522	0.364
G	T1	None	None	9	0.940	0.880	0.090	0.863	0.239	0.860	0.880	0.130	0.716	0.352
		OSC+MC	MC	9	1.000	1.000	0.000	0.965	0.123	0.920	0.960	0.060	0.851	0.258
	T2	None	None	7	0.840	0.920	0.120	0.747	0.313	0.920	0.840	0.180	0.649	0.365
		OSC+MC	MC	5	0.960	0.940	0.050	0.884	0.22	0.800	0.860	0.170	0.682	0.370
	T3	None	None	9	0.800	0.860	0.170	0.681	0.346	0.720	0.680	0.300	0.446	0.444
		OSC+MC	MC	8	1.000	0.960	0.020	0.890	0.215	0.800	0.820	0.190	0.684	0.361
H	T3	None	None	7	0.880	0.600	0.260	0.560	0.393	0.840	0.480	0.340	0.420	0.451
		OSC+MC	MC	2	0.900	0.960	0.070	0.754	0.309	0.840	0.680	0.240	0.519	0.423
	T4	None	None	11	0.680	0.840	0.240	0.587	0.382	0.560	0.720	0.360	0.130	0.575
		OSC+MC	MC	9	0.880	0.920	0.100	0.773	0.299	0.600	0.720	0.340	0.226	0.584
	T5	None	None	7	0.760	0.780	0.230	0.609	0.374	0.720	0.720	0.280	0.422	0.438
		OSC+MC	MC	4	0.880	0.900	0.110	0.771	0.300	0.640	0.780	0.290	0.490	0.444

Table 3. Performance of PLSDA model for evaluation of TT

OSC: Orthogonal signal correction, MC: Mean centering, LV: Latent variable, R_C: Correlation coefficient of calibration, RMSEC: Root mean square error of calibration, R_{CV}: Correlation coefficient of cross-validation, RMSECV: Root mean square error of cross-validation.

Table 4. Performance of full-wavenumber PLSR model for determination of TTP.

Textural parameter	X-block Pre-processing	Y-block Pre-processing	No. LV	Calibration		Cross-validation		Prediction	
				R_C	RMSEC	R_{CV}	RMSECV	R_P	RMSEP
Hardness	None	None	9	0.860	51.832	0.759	66.855	0.766	77.221
	2nd Der	None	13	0.944	33.614	0.771	67.750	0.811	77.688
	OSC	None	8	0.912	41.807	0.791	63.930	0.831	69.713
	MC	None	9	0.869	117.640	0.779	127.158	0.802	142.704
	1st Der+MC	None	9	0.901	115.115	0.796	125.046	0.822	141.592
	OSC+MC	None	8	0.912	114.240	0.794	125.183	0.837	114.470
	MC	MC	9	0.869	50.269	0.771	65.779	0.802	73.593
	1st Der+MC	MC	9	0.901	44.140	0.791	63.670	0.822	69.804
	OSC+MC	MC	8	0.917	40.677	0.796	63.407	0.846	68.029
Resilience	None	None	10	0.864	0.066	0.746	0.091	0.871	0.077
	2nd Der	None	10	0.867	0.065	0.678	0.103	0.754	0.090
	OSC	None	8	0.897	0.058	0.742	0.093	0.873	0.069
	MC	None	9	0.851	0.302	0.752	0.309	0.885	0.251
	1st Der+MC	None	7	0.896	0.300	0.818	0.306	0.876	0.257
	OSC+MC	None	8	0.898	0.300	0.742	0.311	0.871	0.259
	MC	MC	9	0.851	0.069	0.738	0.091	0.885	0.071
	1st Der+MC	MC	7	0.896	0.058	0.809	0.078	0.876	0.072
	OSC+MC	MC	4	0.917	0.052	0.722	0.098	0.893	0.063
Cohesiveness	None	None	8	0.696	0.129	0.545	0.157	0.616	0.133
	2nd Der	None	9	0.814	0.105	0.638	0.148	0.734	0.117
	OSC	None	8	0.670	0.134	0.486	0.166	0.679	0.120
	MC	None	9	0.823	0.424	0.702	0.434	0.643	0.403
	1st Der+MC	None	6	0.825	0.424	0.671	0.437	0.691	0.402
	OSC+MC	None	7	0.812	0.425	0.653	0.432	0.621	0.400
	MC	MC	9	0.823	0.100	0.701	0.127	0.643	0.131
	1st Der+MC	MC	6	0.825	0.097	0.669	0.133	0.691	0.124
	OSC+MC	MC	6	0.891	0.080	0.711	0.129	0.673	0.124
Springiness	None	None	9	0.674	0.096	0.523	0.115	0.489	0.108
	2nd Der	None	9	0.722	0.089	0.336	0.136	0.422	0.110
	OSC	None	8	0.669	0.096	0.523	0.115	0.527	0.104
	MC	None	9	0.679	0.566	0.493	0.568	0.457	0.587
	1st Der+MC	None	9	0.738	0.564	0.490	0.570	0.548	0.593
	OSC+MC	None	10	0.699	0.565	0.489	0.566	0.561	0.588
	MC	MC	9	0.679	0.095	0.481	0.117	0.457	0.107
	1st Der+MC	MC	9	0.738	0.087	0.480	0.119	0.548	0.101
	OSC+MC	MC	9	0.740	0.087	0.468	0.126	0.563	0.101
Gumminess	None	None	9	0.840	32.587	0.746	40.184	0.729	48.715
	2nd Der	None	10	0.876	28.950	0.669	47.053	0.717	50.184
	OSC	None	9	0.897	26.524	0.793	37.353	0.796	44.964
	MC	None	9	0.846	56.944	0.755	62.595	0.766	71.674
	1st Der+MC	None	8	0.873	55.434	0.754	63.151	0.742	74.706
	OSC+MC	None	9	0.902	53.778	0.797	61.078	0.784	73.478
	MC	MC	9	0.846	31.989	0.750	40.111	0.766	46.638
	1st Der+MC	MC	8	0.873	29.217	0.750	40.541	0.742	48.608
	OSC+MC	MC	7	0.903	25.823	0.797	37.086	0.798	44.571
Chewiness	None	None	9	0.850	22.211	0.760	27.602	0.711	38.040
	2nd Der	None	10	0.880	20.097	0.677	32.789	0.717	38.096
	OSC	None	9	0.909	17.583	0.822	24.409	0.797	34.598
	MC	None	9	0.857	37.062	0.771	41.093	0.751	51.205
	1st Der+MC	None	8	0.885	35.839	0.779	41.103	0.731	52.848
	OSC+MC	None	8	0.910	34.686	0.824	38.917	0.785	51.819
	MC	MC	9	0.857	21.785	0.766	27.377	0.751	36.589
	1st Der+MC	MC	8	0.885	19.633	0.776	27.154	0.731	37.603
	OSC+MC	MC	9	0.912	17.358	0.819	24.542	0.791	34.871

2nd Der: Second derivative, OSC: Orthogonal signal correction, MC: Mean centering, 1nd Der: Frist derivative, LV: Latent variable, R_C: Correlation coefficient of calibration, RMSEC: Root mean square error of calibration, R_{CV}: Correlation coefficient of cross-validation, RMSECV: Root mean square error of cross-validation, R_P: Correlation coefficient of prediction, RMSEP: Root mean square error of prediction.

Table 5. Performance of full-wavenumber LWPLSR model for measurement of TTP.

Textural parameter	X-block Pre-processing	Y-block Pre-processing	No. LV	Calibration		Prediction	
				R_C	RMSEC	R_P	RMSEP
Hardness	None	None	9	0.949	32.306	0.843	72.607
	OSC+MC	MC	9	0.970	24.918	0.878	67.844
Resilience	None	None	9	0.962	0.036	0.855	0.058
	OSC+MC	MC	9	0.970	0.032	0.911	0.049
Cohesiveness	None	None	9	0.949	0.056	0.615	0.149
	OSC+MC	MC	9	0.969	0.044	0.666	0.133
Springiness	None	None	9	0.868	0.065	0.520	0.114
	OSC+MC	MC	9	0.920	0.052	0.479	0.124
Gumminess	None	None	9	0.953	18.163	0.766	46.613
	OSC+MC	MC	9	0.970	14.741	0.815	44.972
Chewiness	None	None	9	0.957	12.300	0.756	36.549
	OSC+MC	MC	9	0.975	9.411	0.817	34.883

OSC: Orthogonal signal correction, MC: Mean centering, LV: Latent variable, R_C: Correlation coefficient of calibration, RMSEC: Root mean square error of calibration, R_P: Correlation coefficient of prediction, RMSEP: Root mean square error of prediction.

Table 6. Performance of fingerprint-wavenumber models for determination of TTP.

Textural parameter	Model	X-block Pre-processing	Y-block Pre-processing	No. LV	Calibration		Prediction	
					R_C	RMSEC	R_P	RMSEP
Hardness	PLSR	None	None	8	0.791	62.127	0.740	80.632
		OSC+MC	MC	9	0.899	44.434	0.791	74.098
	LWPLSR	None	None	10	0.962	27.971	0.845	63.701
		OSC+MC	MC	7	0.937	31.51	0.799	72.625
Resilience	PLSR	None	None	10	0.789	0.081	0.804	0.083
		OSC+MC	MC	10	0.873	0.064	0.856	0.082
	LWPLSR	None	None	9	0.960	0.037	0.909	0.069
		OSC+MC	MC	8	0.956	0.039	0.872	0.076
Cohesiveness	PLSR	None	None	9	0.741	0.121	0.787	0.101
		2nd Der	MC	9	0.733	0.124	0.781	0.109
	LWPLSR	None	None	9	0.939	0.061	0.674	0.137
		OSC+MC	MC	9	0.959	0.051	0.609	0.148
Springiness	PLSR	None	None	9	0.547	0.109	0.488	0.11
		OSC+MC	MC	4	0.828	0.099	0.748	0.112
	LWPLSR	None	None	9	0.832	0.072	0.509	0.106
		OSC+MC	MC	4	0.732	0.088	0.562	0.099
Gumminess	PLSR	None	None	8	0.785	37.171	0.736	47.577
		OSC+MC	MC	11	0.901	26.062	0.738	47.761
	LWPLSR	None	None	9	0.939	20.695	0.792	42.776
		OSC+MC	MC	13	0.989	8.734	0.814	41.024
Chewiness	PLSR	None	None	8	0.796	25.54	0.723	36.793
		OSC	MC	9	0.893	19.044	0.695	38.546
	LWPLSR	None	None	9	0.946	13.725	0.741	35.748
		OSC+MC	MC	8	0.963	11.504	0.742	35.668

PLSR: Partial least square regression, LWPLSR: Locally weighted partial least squares regression, OSC: Orthogonal signal correction, MC: Mean centering, LV: Latent variable, R_C: Correlation coefficient of calibration, RMSEC: Root mean square error of calibration, R_P: Correlation coefficient of prediction, RMSEP: Root mean square error of prediction.

Table 7. Performance of feature-wavenumber models using FMCIA for determination of TTP.

Textural parameter	Model	No. LV	Calibration		Prediction	
			R_C	RMSEC	R_P	RMSEP
Hardness	PLSR	7	0.734	69.071	0.640	92.054
	LWPLSR	8	0.937	46.481	0.890	73.645
Resilience	PLSR	9	0.615	0.107	0.581	0.101
	LWPLSR	5	0.891	0.061	0.877	0.060
Cohesiveness	PLSR	10	0.629	0.14	0.546	0.138
	LWPLSR	5	0.787	0.111	0.641	0.128
Springiness	PLSR	9	0.482	0.123	0.356	0.132
	LWPLSR	6	0.686	0.094	0.621	0.092
Gumminess	PLSR	7	0.716	41.875	0.691	51.095
	LWPLSR	8	0.865	30.275	0.743	47.244
Chewiness	PLSR	7	0.736	28.581	0.704	38.233
	LWPLSR	8	0.890	46.481	0.789	73.645

PLSR: Partial least square regression, LWPLSR: Locally weighted partial least squares regression, LV: Latent variable, R_C: Correlation coefficient of calibration, RMSEC: Root mean square error of calibration, R_P: Correlation coefficient of prediction, RMSEP: Root mean square error of prediction.

Figure captions

Fig. 1. The microscopic images of Rooster tuber samples collected by FT-IR imaging system in 5 time periods from (a) 0s to (e) 35s.

Fig. 2. Reference values of textural property of sweet potato Fig. 2(a-f) and red potato Fig. 2(g-l). Error bars represented the standard deviation among five replicates at each time point.

Fig. 3. Raw FT-IR absorption spectra of tuber samples in (a) the full-wavelength range (4000–600 cm^{-1}) and (b) the limited spectral region (1800–900 cm^{-1}).

Fig. 4. The optimal results of PLSDA models for evaluation of spectral property.

Fig. 5. The comparison of original and optimal full wavenumber models for measurement of TTP.

Fig. 6 The performance of the optimal PLSR model (c and d) and LWPLSR model (a, b, e and f) for prediction of TTP.

Fig. 7 (a) Textural property related feature wavenumbers (1468, 1350, 1333, 1315, 1221, 1185, 1160, 1130, 1083, 1026, 985 and 924 cm^{-1}) are indicated by circles using the FMCIA. The variable indexes from 1 to 12 in (b, c and d) represent these feature wavenumbers from 1468 to 924 cm^{-1}. (b) Optimized feature wavenumbers for predicting hardness, gumminess and chewiness are indicated by square marker based on FMCIA-SPA, (c) optimized feature wavenumbers for assessment of resilience and springiness are indicated by square marker based on FMCIA-SPA, (d) optimized feature wavenumbers for measurement of cohesiveness are indicated by square marker based on FMCIA-SPA.

Fig. 8 Performance of FMCIA-SPA-LWPLSR models for determination of TTP.

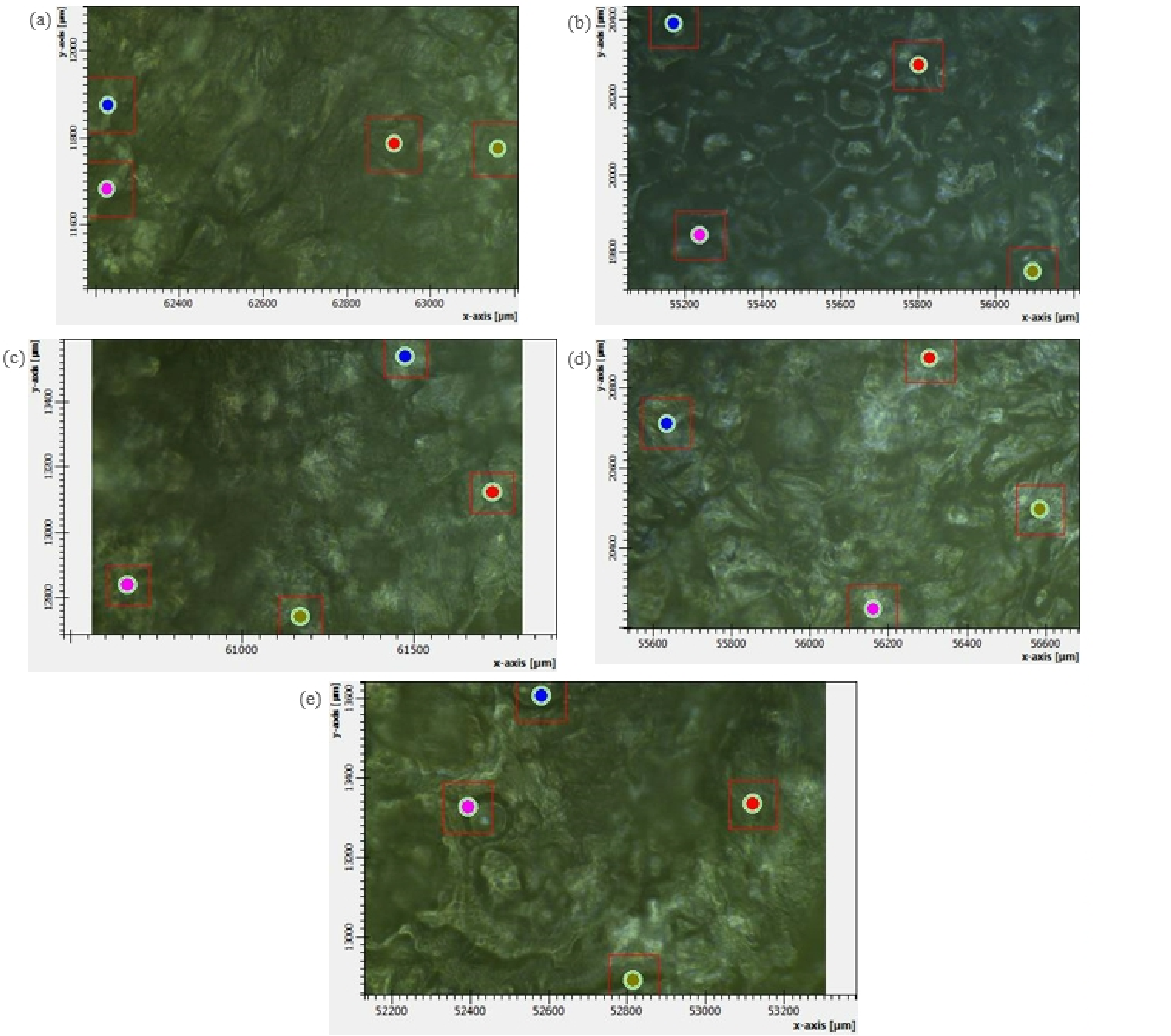

Fig. 1. The microscopic images of Rooster tuber samples collected by FTMIR imaging system in 5 time periods from (a) 0s to (e) 35s.

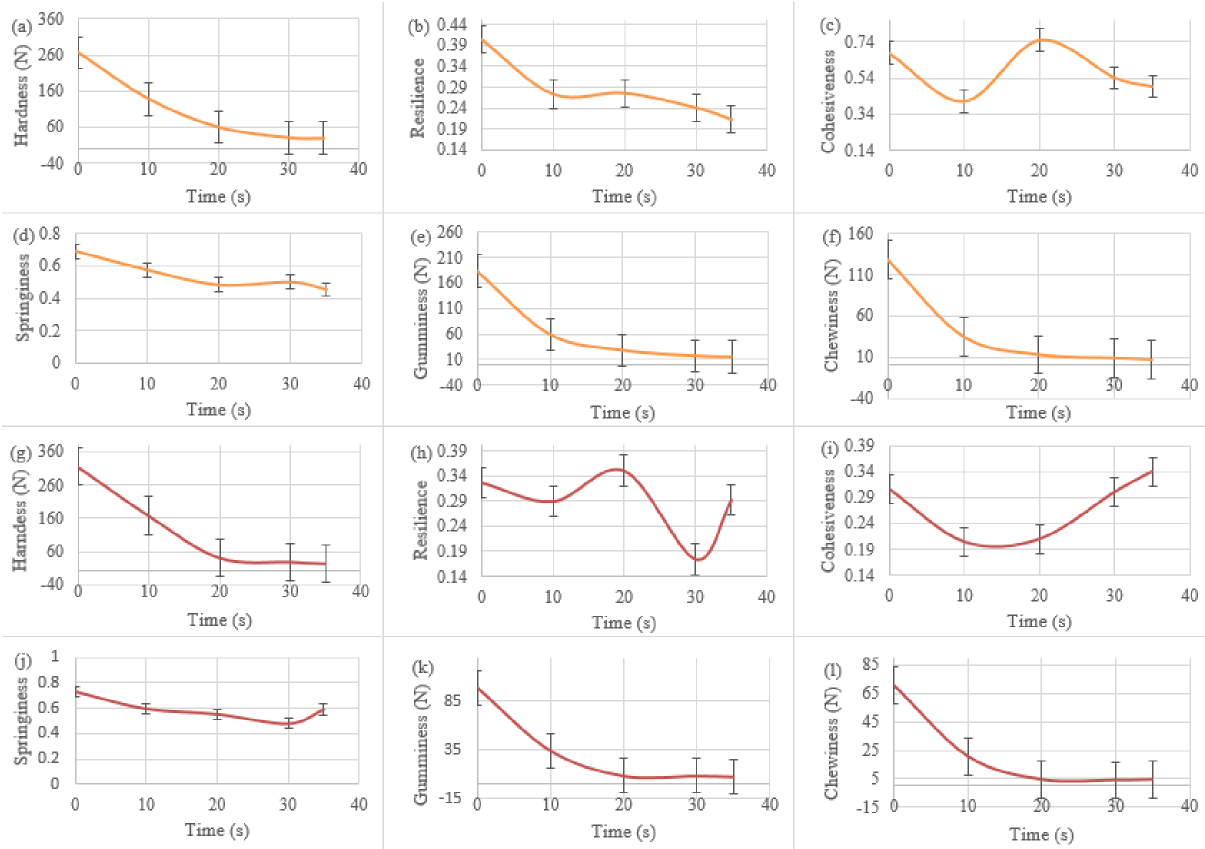

Fig. 2. Reference values of textural property of sweet potato Fig. 2(a-f) and red potato Fig. 2(g-l). Error bars represented the standard deviation among five replicates at each time point.

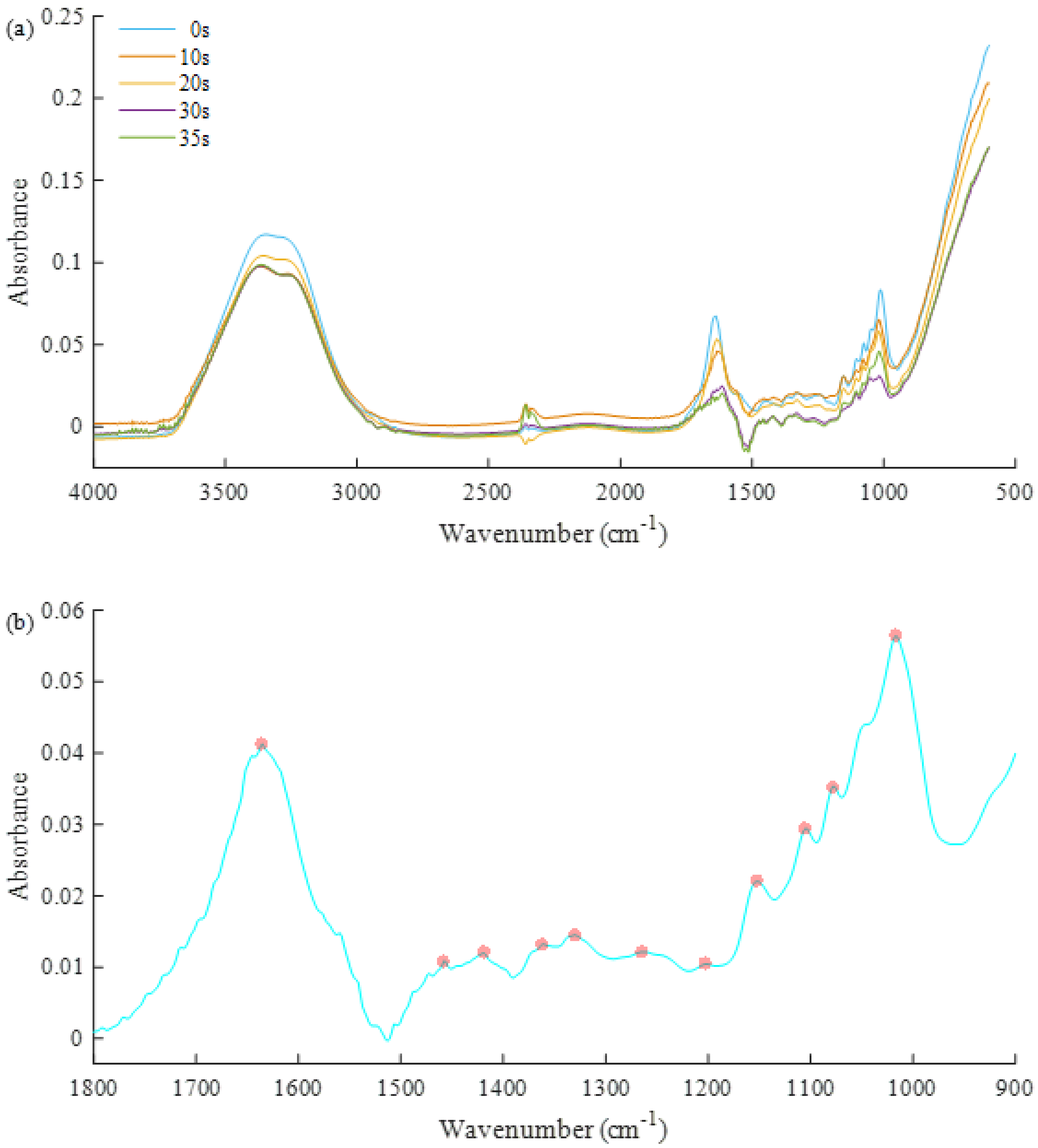

761

762 **Fig. 3.** Raw FT-IR absorption spectra of tuber samples in (a) the full-wavelength range (4000–600
763 cm^{-1}) and (b) the limited spectral region (1800–900 cm^{-1}).

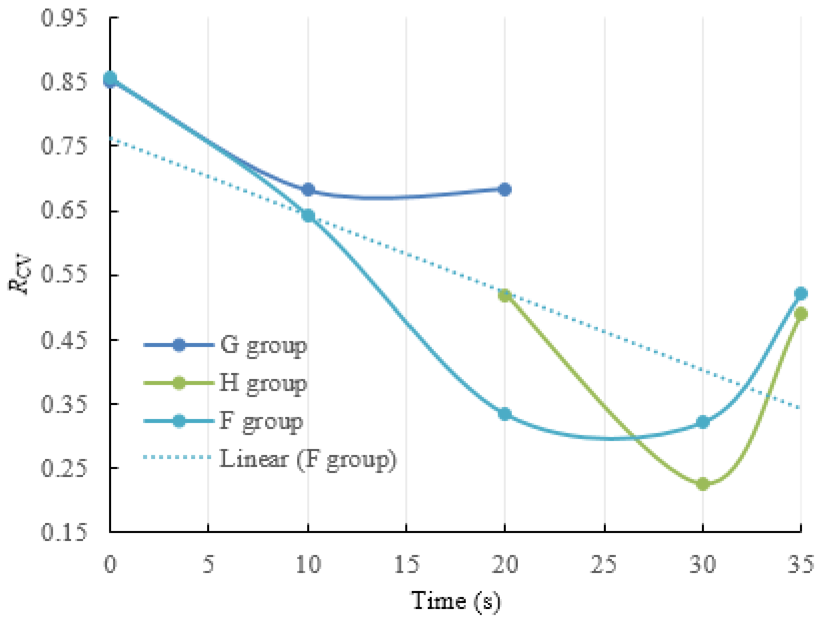

Fig. 4. The optimal results of PLSDA models for evaluation of spectral property.

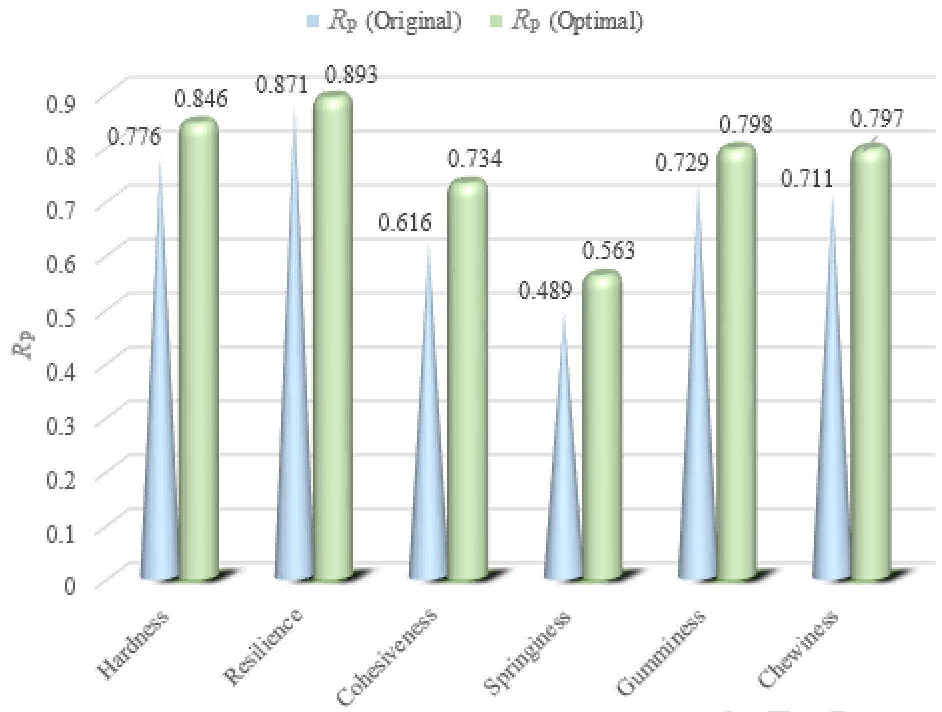

Fig. 5. The comparison of original and optimal full wavenumber models for measurement of TTP.

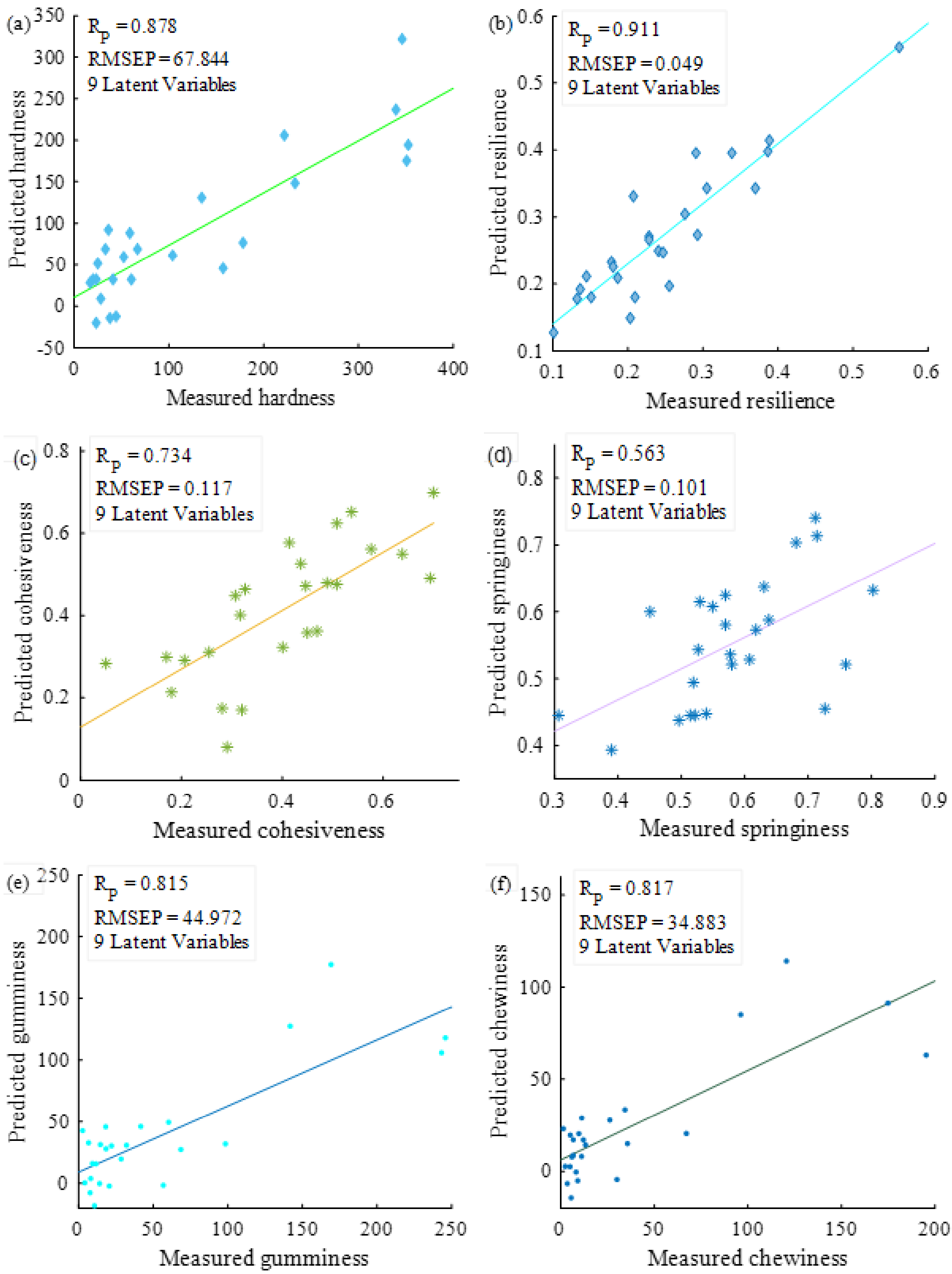

Fig. 6 The performance of the optimal PLSR model (c and d) and LWPLSR model (a, b, e and f) for prediction of TTP.

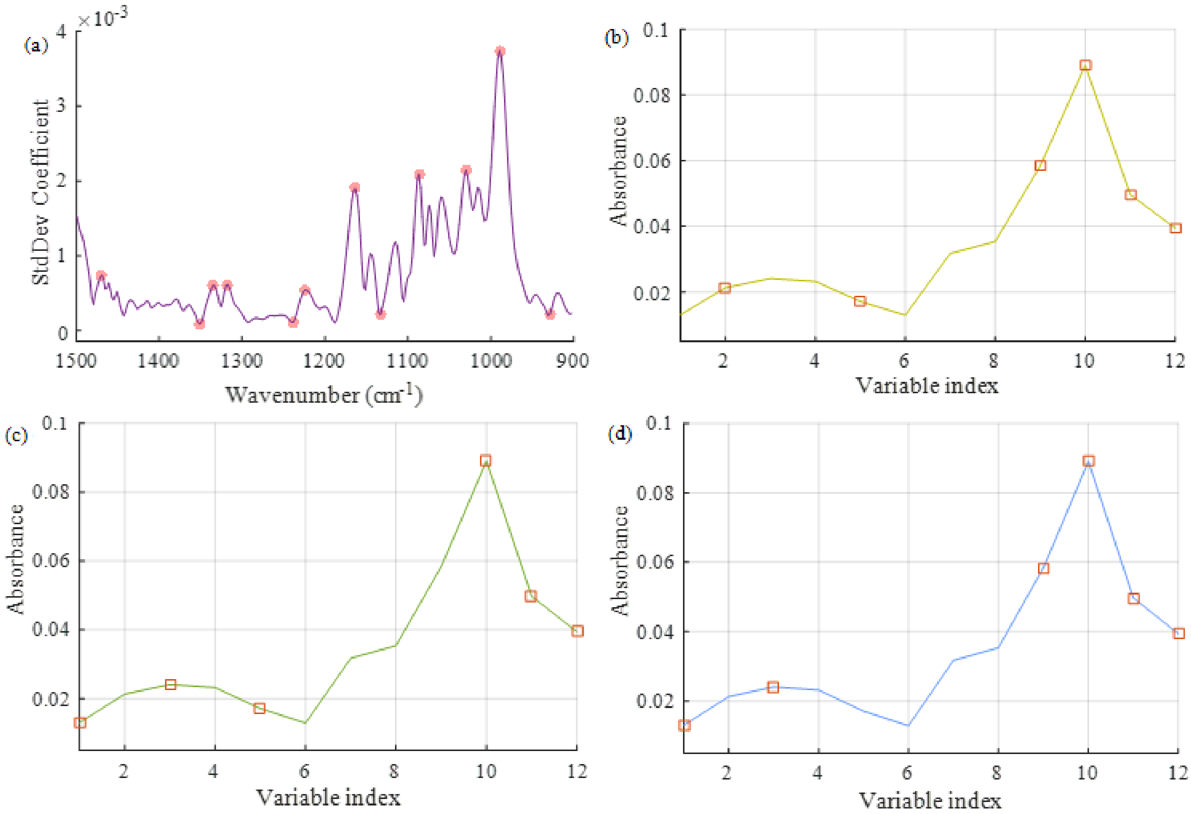

Fig. 7 (a) Textural property related feature wavenumbers (1468, 1350, 1333, 1315, 1221, 1185, 1160, 1130, 1083, 1026, 985 and 924 cm^{-1}) are indicated by circles using the FMCIA. The variable indexes from 1 to 12 in (b, c and d) represent these feature wavenumbers from 1468 to 924 cm^{-1}. (b) Optimized feature wavenumbers for predicting hardness, gumminess and chewiness are indicated by square marker based on FMCIA-SPA, (c) optimized feature wavenumbers for assessment of resilience and springiness are indicated by square marker based on FMCIA-SPA, (d) optimized feature wavenumbers for measurement of cohesiveness are indicated by square marker based on FMCIA-SPA.

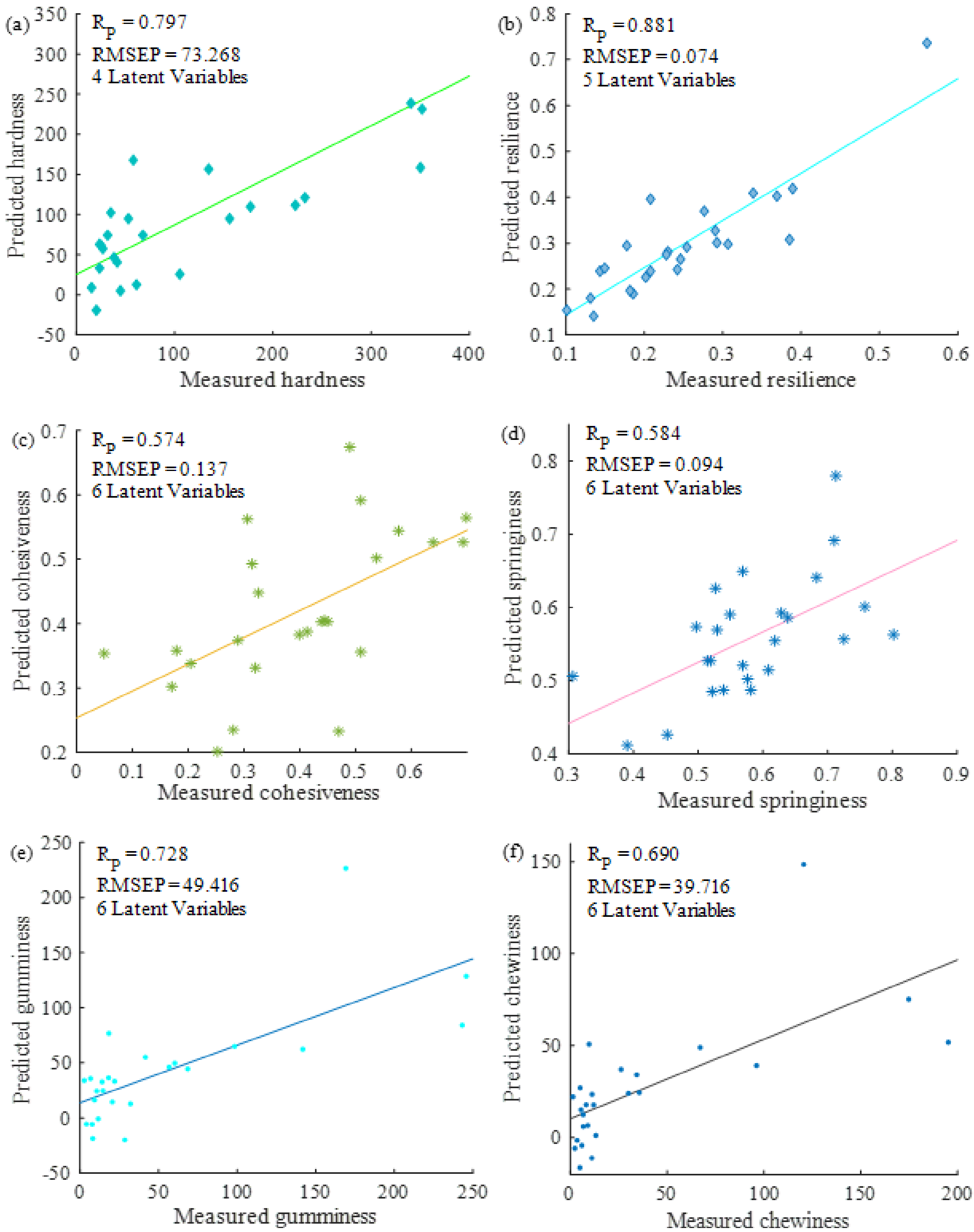

Fig. 8 Performance of FMCIA-SPA-LWPLSR models for determination of TTP.

Highlights

- The mid-infrared spectral property was analyzed based on PLSDA.
- PLSR and LWPLSR models were developed to measure tuber textural property.
- The fingerprint spectra showed better modelling ability for texture detection.
- The FMCIA-SPA is verified as a new approach for feature wavenumber selection.
- Tuber textural property could be detected using mid-infrared spectroscopy.